IOP Publishing Journal of Physics B: Atomic, Molecular and Optical Physics
J. Phys. B: At. Mol. Opt. Phys. **52** (2019) 244001 (10pp) https://doi.org/10.1088/1361-6455/ab4c22

Calculations of long range interactions for ^{87}Sr Rydberg states

F Robicheaux[1,2]

[1] Department of Physics and Astronomy, Purdue University, West Lafayette, IN 47907, United States of America
[2] Purdue Quantum Science and Engineering Institute, Purdue University, West Lafayette, IN 47907, United States of America

E-mail: robichf@purdue.edu

Received 31 July 2019, revised 26 September 2019
Accepted for publication 8 October 2019
Published 12 November 2019

Abstract

A method for calculating the properties of Rydberg states and Rydberg–Rydberg interaction between two ^{87}Sr atoms is described. The method is based on a multichannel quantum defect theory description of the Rydberg states that accounts for the hyperfine splitting of the $^{87}Sr^{+}$ ground state. Results are given for the scalar and tensor polarizabilities and the eigenvalues of the C_6 matrix for the $5sns\ F_T = 9/2$ series. These results illustrate the new features that arise due to the hyperfine splitting of the thresholds. In particular, there should be several couple Förster resonances above $n = 50$ unlike the case of ^{88}Sr which has none.

Keywords: strontium, Rydberg–Rydberg, MQDT, C6

(Some figures may appear in colour only in the online journal)

1. Introduction

The interaction between two Rydberg atoms provides the possibility for entanglement between the electronic states of atoms separated by more than a μm. This possibility arises due to the extreme character of Rydberg states [1]. There is interest [2, 3] in the alkaline earth atoms due to the long lifetime of some excited states as well as the flexibility due to the extra electron. For example, the inner valence electron could be used to match polarizability of the ground and Rydberg state [4–6] which would allow for magic trapping of Rydberg atoms. As another example, the inner electron can be used to probe the status of the Rydberg electron [7, 8].

The purpose of this paper is to elucidate a theory capable of accurate calculation of properties of Rydberg atoms for odd isotopes of Sr. The calculation of Rydberg–Rydberg interactions has progressed from alkali atoms [9, 10] where the core electrons are ^{1}S to even isotopes of alkaline-earth atoms [11, 12] where the core has angular momentum $1/2$ but not hyperfine splitting to the most general case where the core has angular momentum and hyperfine splitting [13]. The odd isotopes of the alkaline earth atoms have nuclear spin I and the positive ions have ground states $F = I \pm 1/2$ with non-zero hyperfine splitting. The results below for ^{87}Sr were obtained by applying the theory in [13]. In some cases, we applied the theory in [11] for $I = 0$ to understand the role of the hyperfine splitting.

Unlike the alkali atoms, several of the Rydberg series of Sr have a complicated dependence on n, even without the hyperfine splitting, due to perturbers attached to the higher lying $4d$ and $5p$ thresholds [12, 14–23]. Because we are interested in the high-n Rydberg states, much of the complications of the two electron states can be subsumed within the machinery of multichannel quantum defect theory (MQDT) [20]. The main parameters needed in the calculations are the energy dependent quantum defects for the different channels. We will use the compilation of quantum defects in [11] and the recent measurements in [22, 23] in all of the calculations. The recent measurements in [22, 23] have improved the quantum defects for some $5sns$ and $5snd$ series at higher n but more accurate values are needed for other series. The biggest need is for measurements of the $5snp$ ^{1,3}P quantum defects at higher n because this would allow accurate calculations of the polarizability and C_6 matrices for the ^{1,3}S series. Because we use ideas from hyperfine frame transformation [13, 16–18, 24], the quantum defects from the even isotopes of Sr are a good approximation in the calculations.

Table 1. Quantum defects used in the calculations. See the text for a discussion of uncertainties in these values.

	μ_0	μ_2	μ_4	Fitted range	References
$^1S_0$	3.268 96(2)	−0.138(7)	0.9(6)	$14 \leqslant n \leqslant 34$	[11]
$^3S_1$	3.370 65	0.443	−0.553	$30 \leqslant n \leqslant 99$	[22]
$^3S_1$	3.370 778(4)	0.418(1)	−0.3(1)	$15 \leqslant n \leqslant 50$	[23]
$^1P_1$	2.7295(7)	−4.67(4)	−157(2)	$10 \leqslant n \leqslant 29$	[11]
$^3P_0$	2.8866(1)	0.44(1)	−1.9(1)	$8 \leqslant n \leqslant 15$	[11]
$^3P_1$	2.8824(2)	0.407(5)	−1.3(1)	$8 \leqslant n \leqslant 22$	[11]
$^3P_2$	2.8719(2)	0.446(5)	−1.9(1)	$8 \leqslant n \leqslant 18$	[11]
$^1D_2$	2.3807(2)	−39.41(6)	−1090(20)	$20 \leqslant n \leqslant 50$	[11]
$^3D_1$	2.673	−5.4	−8166.	$50 \leqslant n \leqslant 98$	[22]
$^3D_1$	2.675 17(20)	−13.15(26)	−4444(91)	$28 \leqslant n \leqslant 50$	[23]
$^3D_2$	2.662	−15.4	−9804.	$50 \leqslant n \leqslant 98$	[22]
$^3D_2$	2.661 42(30)	−16.77(38)	−6656(134)	$28 \leqslant n \leqslant 50$	[23]
$^3D_3$	2.612	−41.4	−15363.	$50 \leqslant n \leqslant 98$	[22]
$^1F_3$	0.089(1)	−2.0(2)	30(2)	$10 \leqslant n \leqslant 25$	[11]
$^3F_2$	0.120(1)	−2.2(2)	120(20)	$10 \leqslant n \leqslant 24$	[11]
$^3F_2$	0.120(1)	−2.2(2)	120(20)	$10 \leqslant n \leqslant 24$	[11]
$^3F_2$	0.120(1)	−2.4(2)	120(20)	$10 \leqslant n \leqslant 24$	[11]

Table 2. Energies for the $5sns$ series. The columns for E are in cm^{-1} and the columns for ΔE are the energy difference to the $5sns$ $^3S_1$ $F_T = 11/2$ state in GHz.

n	Term	F	E_{ex}	ΔE_{ex}	E_{th}[a]	ΔE_{th}[a]	E_{th}[b]	ΔE_{th}[b]	E_{th}[c]	ΔE_{th}[c]
40	$^1S_0$	9/2	45 850.8762(21)	16.35(8)	45 850.8702	16.22	45 850.8743	16.31	45 850.8743	16.32
60	$^1S_0$	9/2	45 898.1444(22)	7.28(9)	45 898.1421	7.26	45 898.1434	7.26	45 898.1433	7.26
82	$^1S_0$	9/2	45 914.5606(22)	5.66(9)	45 914.5589	5.67	45 914.5602	5.67	45 914.5602	5.67
40	$^3S_1$	7/2	45 850.4974(21)	4.99(8)	45 850.4960	5.0	45 850.4972	5.00	45 850.4967	5.00
60	$^3S_1$	7/2	45 898.0688(21)	5.02(9)	45 898.0668	5.0	45 898.0681	5.00	45 898.0680	5.00
82	$^3S_1$	7/2					45 914.5380	5.00	45 914.5379	5.00
40	$^3S_1$	9/2	45 850.4078(21)	2.31(8)	45 850.4061	2.31	45 850.4074	2.31	45 850.4070	2.31
60	$^3S_1$	9/2					45 897.9488	1.42	45 897.9487	1.42
82	$^3S_1$	9/2	45 914.3958(21)	0.72(9)	45 914.3935	0.71	45 914.3947	0.71	45 914.3947	0.71
40	$^3S_1$	11/2	45 850.3308(15)	0	45 850.3291	0	45 850.304	0	45 850.3299	
60	$^3S_1$	11/2	45 897.9014(19)	0	45 897.9000	0	45 897.9013	0	45 897.9011	
82	$^3S_1$	11/2	45 914.3718(22)	0	45 914.3699	0	45 914.3711	0	45 914.3711	

[a] Theory calculations from [22].
[b] MQDT calculations using the ^3S quantum defects from [22] and the ^1S from [11].
[c] MQDT calculations using the ^3S quantum defects from [23] and the ^1S from [11].

The paper is organized as follows. Section 2 gives a description of the method used in the calculations. Section 3 gives results for calculations of ^{87}Sr including energy levels compared to recent measurements [22], scalar and tensor polarizability, and the eigenvalues of the C_6 matrix. Section 4 contains brief conclusions. The units in the different calculations are specified.

2. Methods

In this section, the method for performing MQDT calculations [20] of Rydberg–Rydberg interactions is described. The method is similar to that in [13] but with a different coupling scheme for the channel functions. The coupling scheme for ^{87}Sr is chosen to take advantage of the angular momenta for this atom: there are simplifications for ^{87}Sr because the core electron has total orbital angular momentum $L_c = 0$. The change in channel coupling leads to different details for the MQDT equations compared to those in [13].

The MQDT treatment of the bound states attached to the hyperfine split thresholds is also similar in style to that in [17, 18, 24] but with a different angular momentum coupling. Given the quantum defects in table 1 and the hyperfine splitting, they would obtain the same bound state energies in tables 2 and 3. The main difference from [17, 18, 24] is that they did not give a method for calculating the polarizability and C_6 matrices.

Table 3. Energies for the $5s50d$ states. The columns for E are in cm^{-1} and the columns for ΔE are the energy difference to one level within a scan (the state with $\Delta E = 0$) in MHz.

Term	F	E_{ex}	ΔE_{ex}	E_{th} [a]	ΔE_{th} [a]	E_{th} [b]	ΔE_{th} [b]	E_{th} [c]	ΔE_{th} [c]
$^3D_1$	7/2	45 883.1440(22)	−295.60(7)	45 883.1414	−299.01	45 883.1427	−296.94	45 883.1438	−296.83
$^3D_1$	9/2	45 883.1538(22)	0	45 883.1514	0	45 883.1526	0	45 883.1537	0
$^3D_2$	11/2	45 883.1685(22)	439.39(7)	45 883.1662	443.71	45 883.1673	441.11	45 883.1684	440.75
$^3D_2$	7/2	45 883.2882(21)	0	45 883.2855	0	45 883.2866	0	45 883.2876	0
$^3D_2$	9/2	45 883.2922(21)	118.91(7)	45 883.2893	114.7	45 883.2904	116.20	45 883.2915	114.75
$^3D_1$	11/2	45 883.2972(21)	269.12(7)	45 883.2942	260.55	45 883.2954	263.73	45 883.2963	261.22
$^3D_3$	11/2	45 883.3849(22)	−890.64(7)	45 883.3814	−890.22	45 883.3828	−888.59	45 883.3830	−887.29
$^3D_3$	9/2	45 883.4146(22)	0	45 883.4111	0	45 883.4124	0	45 883.4126	0
$^3D_3$	7/2	45 883.4374(22)		45 883.4339		45 883.4351		45 883.4352	

2.1. ^{87}Sr properties

In the calculations below, we use properties of ^{87}Sr to calculate several Rydberg state energies, polarizabilities, and C_6-matrices. The main properties used are the mass of the $^{87}Sr^+$, the hyperfine splitting of the $^{87}Sr^+$ ground state, and the quantum defects of the different series.

The hyperfine interaction of the ground state was taken to be

$$V_{hf} = a_{5s}\vec{I}\cdot\vec{s}/\hbar \tag{1}$$

with $a_{5s} = -2\pi$ 1.000 473 673 GHz [25], $I = 9/2$, and $s = 1/2$. The $^{87}Sr^+$ ground state has $F = 5$ and $F = 4$ with a splitting $\varepsilon_5 - \varepsilon_4 = 5a_{5s}\hbar$. The negative value of a_{5s} means the ground hyperfine state has $F = 5$ and is approximately 5 GHz below the $F = 4$ hyperfine state. The weighted threshold is 45 932.1956 cm [22].

The mass of $^{87}Sr^+$ was taken from [26] to be $M_{87+} = 86.908\,877\,50u - m_e$ with $u = 1.660\ 539\ 066\ 60 \times 10^{-27}$ kg and $m_e = 9.109\ 383\ 7015 \times 10^{-31}$ kg taken from the CODATA values. The Rydberg constant, R_{87}, was taken to be scaled from the CODATA R_∞ value as $R_{87} = 109\ 737.315\ 681\ 60\ cm^{-1} \times M_{87+}/(M_{87+} + m_e)$.

The MQDT formulas below use the quantum defects of the different LSJ channels as energy dependent quantities. This is somewhat different than the definition used in experimental fits which have the quantum defects taken to be functions of n, the principal quantum number. The quantum defect as a function of n is usually written as

$$\mu(n) = \mu_0 + \frac{\mu_2}{(n-\mu_0)^2} + \frac{\mu_4}{(n-\mu_0)^4}, \tag{2}$$

where the μ_a are constants. MQDT treats these parameters as existing as functions of energy with boundary conditions at $r \to \infty$ determining which energies are allowed. To motivate the conversion, we note that the energy of a Rydberg state n is written as $\varepsilon_n = \varepsilon_{thr} - R_{87}/[n-\mu(n)]^2$ with ε in units of cm^{-1} and ε_{thr} the threshold energy. We will take the quantum defects as a function of energy to be

$$\mu(\varepsilon) = \mu_0 + \eta(\varepsilon)\mu_2 + \eta^2(\varepsilon)\mu_4, \tag{3}$$

where $\eta(\varepsilon) \equiv (\varepsilon_{thr} - \varepsilon)/R_{87}$. Since these two expressions for μ are not equivalent, it seems that the μ_a need to be converted between the two expressions. However, one can show that $1/[n-\mu_0]^2 = 1/[n-\mu(n)]^2$ plus a term of order $1/(n-\mu_0)^5$ which means the μ_a are the same through the orders shown. For calculations requiring the highest accuracy, it may be necessary to refit the values of μ_a in equation (3) but that level of accuracy is not appropriate in the calculations below considering the experimental uncertainty in the μ_a. To give a numerical example, the change in energy of the $5s50d$ $^3D_3$ state, which has the largest μ_2 and μ_4, has magnitude $2.3 \times 10^{-5}\,cm^{-1}$ when using equation (2) versus (3). Compare this to the uncertainty in the measured energy which was 2.2×10^{-3} cm^{-1} [22].

The values for the different quantum defects are given in table 1. Note, there are 3 series that have two values listed: $^3S_1$,$^3D_1$, and $^3D_2$. The values in [22] were obtained from fits to ^{87}Sr Rydberg series while those from [23] were obtained from fits to ^{88}Sr Rydberg series. We compare the results from calculations using the quantum defects of [22, 23] below. All of the other values were taken from the compilation of [11] which fit the energies found in [15, 27–29]; see [11] for a discussion of this process. All of the series from [11] arise from fits to energy levels with $n \leqslant 50$ and several for $n \ll 50$; thus, using these quantum defects involves an extrapolation from the fit range and have larger uncertainty for our calculations than simply from the uncertainty in the μ_a. For example, [22] found differences in the $5snd$ ^3D quantum defects of ∼0.02 from the extrapolated values of [11]; these are series with large energy variation in the quantum defects due to perturbers attached to the $4d$ or $5p$ thresholds. However, the $^3S_1$ quantum defect from [11] matches that from [22, 23] within the stated error bars. Taking a large μ_2, μ_4 as a sign of possible problems for extrapolating the quantum defects, one might suspect that the $^1P_1$ and $^1D_2$ series might have the largest errors in quantum defect for $n > 50$. The quantum defects from [23] have a fit range that goes up to $n = 50$ so these quantum defects are probably not as accurate as the stated uncertainty for $n > 50$.

In addition to the quantum defects, there is a mixing between channels with the same parity and J quantum number. The strongest of these mixings is between the $^1D_2$ and

$^3D_2$ channels. Above $n \sim 50$, we will take the mixing to be constant:

$$\begin{pmatrix} \langle {}^1D_2| \\ \langle {}^3D_2| \end{pmatrix}_{rot} = \begin{pmatrix} \cos\theta & \sin\theta \\ -\sin\theta & \cos\theta \end{pmatrix} \begin{pmatrix} \langle {}^1D_2| \\ \langle {}^3D_2| \end{pmatrix} \equiv \underline{R} \begin{pmatrix} \langle {}^1D_2| \\ \langle {}^3D_2| \end{pmatrix}, \quad (4)$$

where $\theta = -0.14$ radians; more accurate parameterization would include an energy dependence for θ. The right-hand side represents the pure singlet and triplet states. These channels are relatively strongly mixed due to a perturber near $n = 15$, but other channels (e.g. $^3S_1$ and $^3D_1$) should be mixed as well. In our calculations, we only included the mixing between $^1D_2$ and $^3D_2$. This type of mixing will probably need to be included for the other channels to obtain the highest accuracy of the Rydberg series.

2.2. Overview MQDT

Section 2 of [13] gives the details for how to determine the bound state energies, polarizabilities, C_6 matrices, etc for Rydberg states attached to hyperfine split thresholds. Refer to this paper for intermediate steps in the formulas given in this section. For a given K-matrix, the bound states, b, are determined by finding the energies, ε_b, that allow for the solution of

$$\sum_i (\tan(\beta_{i,b})\delta_{i',i} + K_{i',i}) \frac{\cos(\beta_i)}{\nu_i^{3/2}} A_{i,b} = 0. \quad (5)$$

with $\beta_{i,b} = \pi(\nu_{i,b} - \ell_i)$ and the effective quantum number in channel i, $\nu_{i,b}$, is defined by $\varepsilon_b = \varepsilon_{c,i} - 2R_{87}/[2\nu_{i,b}^2]$ with $\varepsilon_b - \varepsilon_{c,i}$ being the difference between the total energy and the energy of the ith core state in cm^{-1}. In practice, we solve for ε_b by finding when the determinant of the matrix given by $M_{i'i} = \delta_{i'i}\sin(\beta_i) + K_{i'i}\cos(\beta_i)$ goes through zero. This determines the bound state energy ε_b and allows for a solution of equation (5) for $A_{i,b}$. When the quantum defects vary slowly with energy, the normalization condition is

$$\sum_i A_{i,b}^2 = 1 \quad (6)$$

to a good approximation. With these definitions, the bound state wave function can be written as

$$|\psi_b\rangle = \sum_i |\Phi_i\rangle P_{\nu_i \ell_i}(r) A_{i,b}, \quad (7)$$

where the Φ_i is the channel function which represents all of the quantum numbers except the radial function of the Rydberg electron which goes to 0 at infinity:

$$P_{\nu_i \ell_i}(r) = [f_i(r)\cos\beta_i + g_i(r)\sin\beta_i]/\nu_i^{3/2}, \quad (8)$$

where atomic units are used for r and energy in the f, g radial Coulomb functions.

2.2.1. Frame transformation. The K-matrix is obtained by using a frame transformation on the *LSJ* K-matrix. Adhering as much as possible to the notation of [13], the coupling when the Rydberg electron is close to the core is written as

$$|in\rangle \equiv |(((J_c s_o)S\ell_o)JI)F_T M_T\rangle, \quad (9)$$

where $J_c = 1/2$ is the total core angular momentum, $s_o = 1/2$ is the spin of the Rydberg electron, S is the total spin of the two electrons, ℓ_o is the orbital angular momentum of the Rydberg electron, J is the total angular momentum of the two electrons, $I = 9/2$ is the spin of the nucleus, and F_T, M_T is the total hyperfine angular momentum and its z-projection. This symbol is read by starting from the innermost '( )' and working out. In words, this ket symbolizes: the total angular momentum of the core is coupled to the spin of the Rydberg electron to give total spin S which is coupled to the orbital angular momentum of the Rydberg electron to give total electronic angular momentum J which is coupled to the spin of the nucleus to give the total hyperfine angular momentum F_T and projection M_T. An example case is $|(((1/2,\ 1/2)1,\ 2)3,\ 9/2)13/2,\ 5/2\rangle$ meaning a $5snd$ $^3D_3$ coupled with $I = 9/2$ to give $F_T = 13/2$, $M_T = 5/2$. As with [13], we obtain the final channel functions using two recouplings. The first is

$$|out(1)\rangle = |(((J_c s_o)SI)\bar{F}\ell_o)F_T M_T\rangle, \quad (10)$$

where $\bar{F}$ is a dummy angular momentum arising from coupling the total spin of the electrons to the spin of the nucleus. As with the previous ket, this symbol is read by starting from the innermost '( )' and working out. The second is

$$|out(2)\rangle = |(((J_c I)F_c s_o)\bar{F}\ell_o)F_T M_T\rangle, \quad (11)$$

where F_c is the hyperfine quantum number of the core. The recoupling matrix arises from projecting the different couplings onto each other. The first recoupling matrix is

$$\langle in|out(1)\rangle = (-1)^{\Lambda_{io}}[J, \bar{F}] \begin{Bmatrix} \ell_o & S & J \\ I & F_T & \bar{F} \end{Bmatrix}, \quad (12)$$

where $\{...\}$ is the 6-j symbol, $\Lambda_{io} = \ell_o + \bar{F} - J - I - 2F_T$ and $[a,\ b,\ldots] = \sqrt{(2a+1)(2b+1)\ldots}$. The second recoupling matrix is

$$\langle out(1)|out(2)\rangle = (-1)^{\Lambda_{oo}}[S, F_c] \begin{Bmatrix} s_o & J_c & S \\ I & \bar{F} & F_c \end{Bmatrix}, \quad (13)$$

where $\Lambda_{oo} = s_o + F_c - S - I - 2\bar{F}$. Equations (3.5.14) and (6.1.5) of [30] were used in both projections.

The K matrix is obtained by a series of rotations. For example

$$K_{out(1),out(1)'} = \sum_{in,in'} \langle out(1)|in\rangle K_{in,in'} \langle in'|out(1)'\rangle. \quad (14)$$

A similar rotation is performed to obtain the K-matrix in the $|out(2)\rangle$ coupling scheme. The channel rotation in equation (4) can be taken into account by using the rotated transform

$$\begin{pmatrix} \langle in(^1D_2)_{rot}|out(1)\rangle \\ \langle in(^3D_2)_{rot}|out(1)\rangle \end{pmatrix} = \underline{R} \begin{pmatrix} \langle in(^1D_2)|out(1)\rangle \\ \langle in(^3D_2)|out(1)\rangle \end{pmatrix}. \quad (15)$$

By including this rotation, the K-matrix in equation (14) simplifies to a diagonal matrix:

$$K_{out(1),out(1)'} = \sum_{in} \langle out(1)|in\rangle K_{in} \langle in|out(1)'\rangle \quad (16)$$

with $K_{in} = \tan\pi\mu_{in}$.

2.2.2. Matrix elements. In [13] equation (17), the one electron matrix elements, $Q^{(kq)}_{b,b'}$, determine the polarizability, C_5 matrix, and C_6 matrix [10, 31–33]. These properties require the calculation of matrix elements between bound states b, b'. For these parameters, the operator mainly acts on the Rydberg electron. These cases have an operator of the form $\hat{Q}^{(kq)} = r^k Y_{k,q}(\Omega)$ which has a contribution of size $\sim n^{2k}$ when it acts on the Rydberg electron and of size ~ 1 when it acts on the core electron. In the following, we only account for the contribution to the matrix element from the Rydberg electron. For this approximation, the matrix element is

$$Q^{(kq)}_{b,b'} = \sum_{i,i'} (A^T)_{b,i} \langle \Phi_i | Y_{kq} | \Phi_{i'} \rangle R^{(k)}_{ib,i'b'} A_{i',b'}, \tag{17}$$

where the radial integral is

$$R^{(k)}_{ib,i'b'} = \int_0^\infty dr r^k P_{\nu_{i,b}\ell_i}(r) P_{\nu_{i',b'}\ell_{i'}}, \tag{18}$$

with the radial function defined in equation (8).

For the results below, we are only interested in the dipole matrix elements, $k = 1$. The angular matrix element, equation (19) and (20) of [13], is changed due to the difference in recoupling. Using the channel coupling of equation (11), the angular part of the matrix element is

$$\langle \Phi_i | Y_{kq} | \Phi_{i'} \rangle = \langle ((F_c s_o) \bar{F} \ell_o) F_T M_T | Y_{kq} | ((F'_c s_o) \bar{F}' \ell'_o) F'_T M'_T \rangle, \tag{19}$$

where $J_c = J'_c$ and $I = I'$ automatically hold for ^{87}Sr. The angular matrix element can be evaluated using equations (5.4.1), (5.4.5), and (7.1.8) of [30] to obtain

$$\begin{aligned} \langle \Phi_i | Y_{kq} | \Phi_{i'} \rangle = (-1)^\Lambda \delta_{F_c F'_c} \delta_{\bar{F}\bar{F}'} \frac{[F_T, F'_T, \ell_o, \ell'_o, k]}{\sqrt{4\pi}} \\ \begin{pmatrix} F_T & k & F'_T \\ -M_T & q & M'_T \end{pmatrix} \begin{pmatrix} \ell_o & k & \ell'_o \\ 0 & 0 & 0 \end{pmatrix} \\ \begin{Bmatrix} \ell_o & F_T & \bar{F} \\ F'_T & \ell'_o & k \end{Bmatrix}, \end{aligned} \tag{20}$$

where (...) is the 3-j symbol and $\Lambda = 2F_T - M_T + \bar{F} + \ell_o + \ell'_o + k$. The first 3-$j$ symbol restricts $M_T = M'_T + q$ and $|F_T - F'_T| \leqslant k$. The second 3-j symbol restricts $|\ell_o - \ell'_o| \leqslant k$ and $\ell_o + \ell'_o + k$ to be an even integer.

These expressions can be used in equations from [13] to obtain the C_5 matrix (equation (40)), the C_6 matrix (equations (42) and (43)), and the polarizability matrix.

2.2.3. Approximations. This section discusses some of the approximations that arise from the MQDT method and our implementation of it.

The uncertainty in the threshold splitting and Rydberg constant are too small to be important. The average threshold energy affects where the states appear in a spectrum but does not affect any of the other properties (e.g. polarizability or C_6).

The actual values of the quantum defects are important and uncertainty in the experimental values was discussed above, but an important aspect was not discussed. Except for [22], the quantum defects were measured in isotopes that were not ^{87}Sr. There should be an isotope shift to the quantum defects which will lead to errors in the calculation of properties of the ^{87}Sr Rydberg states. There has not been a discussion of how the quantum defects change with small changes in the mass of the ion. It is reasonable to assume the change in quantum defect is proportional to the change in reduced mass. Thus, measurements in ^{86,88}Sr will have differences of magnitude $\sim 1/(87 \times 1836) = 6.3 \times 10^{-6}$ but opposite sign from ^{87}Sr. Averaging the quantum defects from ^{86,88}Sr will cancel the first order error and give errors of roughly the square of this quantity. Using the data from table 1, the $5s50s\ ^3S_1$ state has quantum defect of 3.370 85 for ^{87}Sr [22] and 3.370 97 for ^{88}Sr [23] which is a difference of magnitude 1.2×10^{-4}. It is not clear to us that this difference is real because the $^3S_1$ energies in table 2 agree to all digits *measured* in [22].

The frame transformation method is an approximation when the quantum defects have energy dependence. The error enters through the change in quantum defect over an energy range $\sim 1/2$ that of the threshold splitting. For ^{87}Sr, this energy is 3.8×10^{-7} a.u. Taking the most rapidly varying quantum defects, it would be like an error of $\sim 3 \times 10^{-5}$ in the μ_0 for the nd series and a factor of 100 smaller for the ^{3}S series.

In the calculation of matrix elements, there should be terms containing the derivative of the quantum defect with respect to energy [20]. The relative size of the error is roughly $d\mu/dE/(d\nu/dE) = d\mu/dn$. This is roughly $2\mu_2/(n - \mu_0)^3 + 4\mu_4/(n - \mu_0)^5$. The worst cases would be the nd series. Taking $n = 50$ would give an error of $\sim 0.1\%$ for ^{1}D and $^3D_3$ which are the largest.

Lastly, while $P_{\nu\ell}(r)$ is finite and well defined outside of the core region, this form does not hold all of the way to $r = 0$. How to treat the radial dependence at small r introduces uncertainty in the calculation. However, the small r part of the radial function contributes very little to the matrix elements of Rydberg properties like polarizability, C_5 matrix, and C_6 matrix. We tried two methods for extending the radial function to $r = 0$ and found they resulted in the same value of the matrix element to better than 0.1%. In both methods, we solved the radial Schrödinger equation from large r to 0 using a Numerov algorithm. In one method, we used a model radial potential developed for Rb and in the other we used a pure $-1/r$. We stopped the Numerov algorithm at a small r when the semiclassical turning point, r_p, was reached; the semiclassical turning point used $(\ell + 1/2)^2/2r^2$. For $r < r_p$, the $P(r) = (r/r_p)^{\ell+1}[P(r_p) + C \times (1 - r/r_p)]$ which automatically gives a continuous $P(r)$. The C was chosen to give a continuous derivative as well. We believe the method that used the Rb model potential was more accurate.

3. Results

This section presents various results for the hyperfine Rydberg states of ^{87}Sr. We have calculated the energies, polarizabilities,

and C_6 matrices for several different series. In this section, we compare the calculated energies to those measured in [22]. We also present examples of the polarizability for the $5sns\ F_T = 9/2$ series. In the last section, we present C_6 coefficients for the pair states [$(5sns,\ F_T = 9/2)$, $(5sns,\ F_T = 9/2)$].

3.1. One atom energies and mixings

This section discusses properties of the Rydberg states of a single atom for different n. Reference [22] measured several energies for $5sns$ and $5snd$ states. From these energies, they fit the quantum defects for the $^3S_1$ and ^3D series. They also performed calculations using a two electron model of the Hamiltonian. Tables 2 and 3 show a representative comparison of their measured and their calculated energies (marked by superscript 'a' in the tables) for a few of the Rydberg states they measured. Also shown are the energies calculated using the MQDT quantization condition, equation (5), using two sets of quantum defects: columns marked with superscript 'b' are the quantum defects from [11, 22] and columns marked with superscript 'c' use the $^3D_3$ from [22], the ($^3S_1$,$^3D_1$,$^3D_2$) from [23], and the rest from [11]. In table 2, the ΔE is the energy difference from the corresponding $5sns\ ^3S_1\ F = 11/2$ state in GHz. In table 3, the ΔE is simply the energy difference between the close states in each group.

For all of the lines, the MQDT calculations are in better agreement with the experiment than the calculations in [22]. There are only two lines where one of the MQDT calculations is outside of the experimental error bars ($5s50d\ ^3D_3\ F = 7/2$ using the [11, 22] quantum defects and $5s40s\ ^3S_1\ F = 11/2$ using [23] quantum defects) whereas the [22] calculations are outside of the error bars for $\sim 1/2$ the levels in the tables and substantially outside of the error bars for a couple of lines.

The extrapolated values for the ^1S series agrees with the measured lines indicating the quantum defects for this series are accurate outside of the fit range. The quantum defects from [23] tend to give $5snd$ energies in better agreement with the measured lines of [22] than the quantum defects from [22]. It is not clear whether this observation is significant because both sets of quantum defects give energies within the experimental uncertainties.

Finally, the splittings of the $5s50d$ states suggests there is some room for improvement of the quantum defects. While the MQDT calculations reproduce the main splitting there are errors at the few MHz level whereas the experimental uncertainty is $\sim$70 kHz.

3.2. One atom perturbations in the even series

One of the interesting aspects of the hyperfine split thresholds is that there can be interesting perturbations between the different Rydberg series of one atom with the same parity and F_T. This can arise when the Rydberg states attached to the $F = 4$ threshold become nearly degenerate with those attached to the $F = 5$ threshold. As an example of this, the two $5sns\ F_T = 9/2$ series are shown in figure 1. The y-axis is proportional to a simulated absorption oscillator strength where only transition into the ^3S character is allowed. The

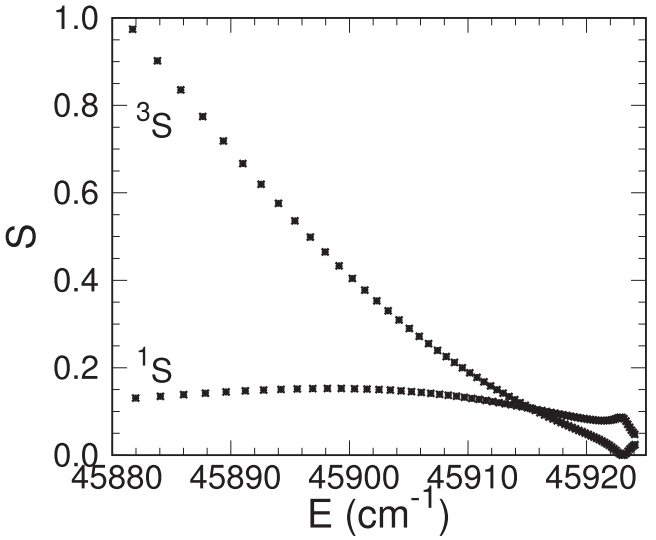

Figure 1. A simulated absorption oscillator strength for the two $5sns$ $F_T = 9/2$ series where only transition into the ^3S character is allowed. Each $*$ represents a Rydberg state. The range shown is from $n \simeq 50$ to $\simeq 120$. For small n, there are two states for each n. At the highest energies shown, it is more useful to think of one Rydberg series attached to each hyperfine threshold.

largest oscillator strength has been normalized to $\sim$1. Near $n = 50$, the state mainly composed of ^3S character and that mainly composed of ^1S character are clearly identified by the size of the oscillator strength. As n increases, there is an overall decrease in oscillator strength proportional to $1/n^3$. However, because of the interaction between the two series, there is an interesting trend where the oscillator strength of the '^1S' series actually increases to $n \sim 60$ because of the increased interaction between the series. Near $n \simeq 110$, there is a nearly complete cancellation in the oscillator strength of one of the series. This near zero arises because the difference in ν between the two channels is 1 at that energy; when this condition occurs, the channels behave as pure ^1S and ^3S channels and the ^1S channel has 0 oscillator strength in the calculation.

This suggests that there is strong mixing within the series below $n = 110$. As an estimate, one can set the condition that the ν state attached to the upper threshold to be equal in energy to the $\nu + 1/2$ state attached to the lower threshold as the condition for strong interaction:

$$\Delta\varepsilon = \frac{1}{2\nu^2} - \frac{1}{2(\nu + 1/2)^2} \simeq \frac{1}{2\nu^3} \tag{21}$$

which gives $\nu \sim 87$. This condition comes from a classical argument: when the Rydberg period is $1/2$ that of the core state, the Rydberg electron interacts with a different F_c each time it returns to small r. (Oddly, when the Rydberg period matches that of the core state, the Rydberg electron interacts with the same F_c each time it returns to small r which is like having no hyperfine splitting at all!) This estimate does not take into account the difference in quantum defects of the different series. This is roughly where the oscillator strength

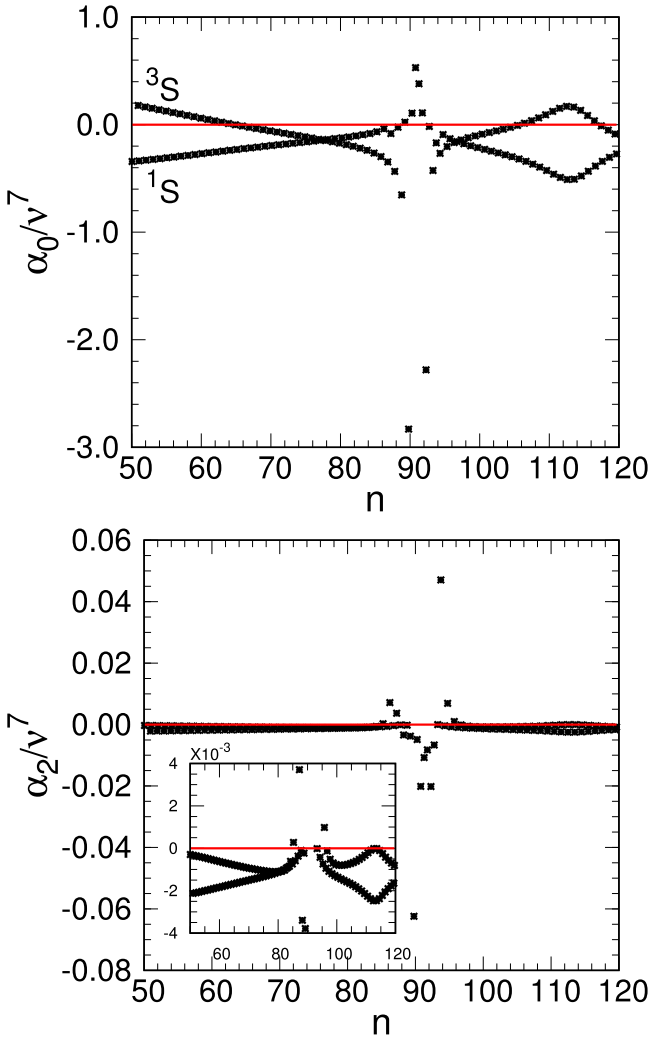

Figure 2. The scalar, α_0, and tensor, α_2, polarizability for the 5*sns* $F_T = 9/2$ states as a function of $n \equiv \nu + 3.32$. The ν is calculated from the hyperfine averaged threshold. The solid (red) line shows $\alpha_0 = 0$.

in the two channels are equal, $n \simeq 81$, which is the condition for the states to have equal mixture of ^{3}S and ^{1}S character.

3.3. One atom polarizability of the 5sns $F_T = 9/2$ series

The polarizability of a Rydberg state determines the coefficient of the quadratic shift of the energy with the strength of a static electric field, $\mathcal{E}$. The shift arises from second order perturbation theory and, for states with non-zero angular momentum, has the form

$$\Delta E = -\frac{1}{2}\left(\alpha_0 + \frac{3M^2 - F(F+1)}{F(2F-1)}\alpha_2\right)\mathcal{E}^2, \qquad (22)$$

where α_0, α_2 are the scalar and tensor polarizabilities, F is the total angular momentum of the state and M is its projection on the z-direction. For simple series, the α_0, α_2 scale like ν^7 because the dipole matrix elements scale like ν^2 and the energy difference scales like $1/\nu^3$: there is the product of two dipole matrix elements in the numerator and the energy difference in the denominator.

We calculated the scalar and tensor polarizability for the 5*sns* $F_T = 9/2$ series with the results shown in figure 2. To avoid the difficulty of two thresholds, the ν is defined relative to the weighted average of the thresholds. The results are plotted versus $n \equiv \nu + 3.32$ which is approximately the principal quantum number of the Rydberg states; the 3.32 was obtained by averaging the μ_0 for the ^{1}S and ^{3}S series. For $n \sim 50$, the states have dominant ^{3}S or ^{1}S character and have been labeled for the scalar polarizability.

There are a few interesting features worth noting. For almost the full range shown, the scalar polarizability is roughly 100× larger than the tensor polarizability. This is because the electric field mainly acts on the spatial dependence of the Rydberg electron which has *S*-character. For $n \simeq 65$, 105, and 117, the scalar polarizability smoothly changes sign which leads to one of the states having its scalar polarizability much smaller than expected; a small scalar polarizability means the state is relatively insensitive to static electric fields. Finally, there are a few states near $n = 90$ that have especially large polarizabilities. This arises through the near degeneracy with 5*snp* states which allows for strong mixing and shifts with small electric fields. All of these *n*-dependent features arise due to the hyperfine splitting of the thresholds. We did a calculation where the hyperfine splitting was artificially reduced by a factor of 100. We found that the polarizability of both series smoothly evolved with *n*. For example, α_0/ν^7 for the ^{1}S series smoothly changes from −0.43 at $n = 50$ to −0.51 at $n = 120$ (when the hyperfine splitting is reduced by a factor of 100, the ^{1}S polarizability is reproduced to better than 1% by the expression $\alpha_0/\nu^7 = -0.57 + 6.5/\nu$ over the range from $n = 50$ to 120).

Because the quantum defects for the 5*snp* states are not known as well as for the 5*sns*, the actual values of the polarizabilities near $n = 90$ are probably not very accurate. However, the way the energy differences change with *n* will be similar. Thus, the results in figure 2 should have the same general features of real ^{87}Sr.

3.4. Two atom C_6 eigenvalues: identical 5sns $F_T = 9/2$ states

This section discusses the Rydberg–Rydberg interaction between a pair of ^{87}Sr atoms. For Rydberg states with outer *s*-electron, the C_5 matrix is identically zero. The first non-zero long range interaction is from the C_6 matrix. The eigenvalues of the C_6 matrix scale like ν^{11} when the states are part of a simple Rydberg series. There is a product of 4 dipole matrix elements in the numerator (giving ν^8) divided by an energy difference (giving a factor of ν^3).

Reference [11] found that the ^{88}Sr C_6 coefficient for the 5*sns* ^{1}S series was negative and smoothly varying between $n = 30$ and 70 while that for the ^{3}S series was somewhat larger in magnitude, positive, and smoothly varying as well. We do find that the C_6 coefficient for the 5*sns* ^{1}S series was negative near $n = 50$ while that for the 5*sns* ^{3}S series was positive near $n = 50$ and somewhat larger in magnitude. However, at larger *n*, the ^{87}Sr 5*sns* series are complicated by

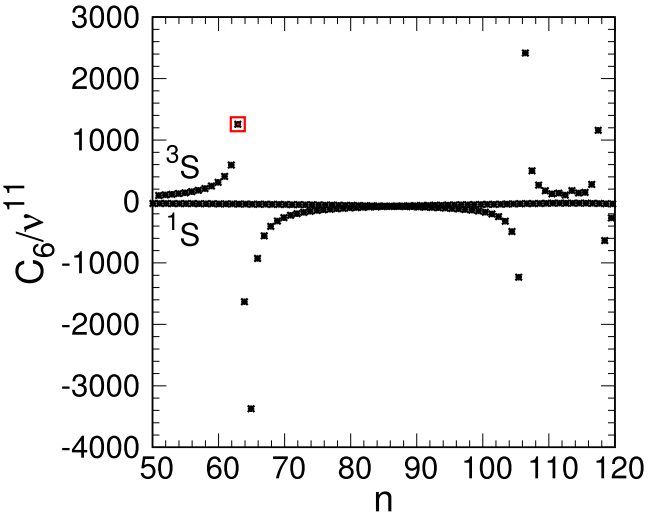

Figure 3. For $F_{T1} = F_{T2} = 9/2$, the scaled C_6 coefficient as a function of $n \equiv \nu + 3.32$ for $M_T = 9$, i.e. the stretched state. The value enclosed by a (red) square is for the $5s63s$ ^{3}S state. To convert to GHz μm^6, multiply by 1.44×10^{-19}.

the threshold splitting and by the non-zero angular momentum of the states due to $I \neq 0$.

We define $F_T = F_{T1} + F_{T2} = 2F_{T1}$ since the calculations are only for identical states. In our calculations, we take the atoms to be separated along a line in the z-direction which means the total z-component of the angular momentum, $M_T = M_{T1} + M_{T2}$, is conserved. Because we are only treating identical states with identical atoms, there are even states and odd states upon swap between the atoms. Also, the symmetry of these states means the eigenvalues for M_T are the same as for $-M_T$. For a given M_T, the number of even states is $1 + \mathrm{mod}(F_T - |M_T|, 2)$ while the number of odd states is $\mathrm{mod}(F_T - |M_T| + 1, 2)$.

Results are presented for the C_6 matrix for identical states with $5sns$ character and $F_{T1} = F_{T2} = 9/2$. These are the mixed ^{3}S and ^{1}S series. The case where $M_T = F_T = 9$ is the stretched state and only has one eigenvalue. The scaled C_6 coefficient for this case is plotted in figure 3. The strong increases in the C_6 near $n \sim 64$ and 105 is due to near degeneracy with $[(5snp), (5sn'p)]$ pair states which arises from the hyperfine splitting of the thresholds: when we decreased the threshold splitting by a factor of 100, the scaled C_6 coefficient was slowly varying over this range. The smooth C_6 for tiny hyperfine splitting reproduces the trends in [11]: they found smoothly varying C_6 for the $5sns$ series in this range of n. The only Förster resonance they showed was for the $5snp$ ^{3}P$_1$ series near $n = 30$ due to interaction with the $5sns$ ^{3}S series which arises because of the energy dependence of the quantum defects.

The C_6 for the $M_T = F_T = 9$ $5s63s$ ^{3}S state is 4.23×10^{22}. All of the contributions are from $5snp$ $F_T = 7/2$, $9/2$, or $11/2$ states Of the 4.23, 1.31 is from two $9/2$ states, 1.06 is from a $9/2$ and a $11/2$ state, and 0.65 is from two $11/2$ states. The rest of the contribution is from many other pairs. Second order perturbation theory, which leads to the C_6, is only relevant when the coupling is smaller than the energy difference. For this state, the coupling equals the energy difference at a separation of 6.4 μm. At a separation of 10 μm, the shift from the C_6 would be 6.1 MHz and the coupling would be $1/4$ of the splitting.

The C_6 eigenvalues for all M_T are shown in figure 4 for a pair of $5s50s$ ^{1}S states, a pair of $5s50s$ ^{3}S states, and a pair of $5s63s$ ^{3}S states. The $5s63s$ ^{3}S states correspond to the point enclosed by the (red) square in figure 3. The C_6 for the $5s64s$ and 65 ^{3}S states are larger but probably less accurate due to the smaller energy difference with the np states. Because the atoms are identical there are even states and odd states upon swap between the atoms. There are some interesting features worth noting. The first is that the spread in eigenvalues of the C_6 matrix is smallest for the pair of $5s50s$ ^{1}S states. Perhaps, this is not surprising because the ^{1}S states are only in the $F_T = 9/2$ series and their isotropic nature is preserved for $n \sim 50$. Another interesting feature, that was also found in [13], is that some of the even and odd states become nearly degenerate when $M_T \to 0$. For the $5s50s$ ^{1}S states, all of the odd states are nearly degenerate with an even state for $M_T \leqslant 7$. For the $5s50s$ ^{3}S states, only the lowest two odd states become nearly degenerate with even states as $M_T \to 0$. This effect is not present at all for the $5s63s$ ^{3}S states which may be due to the near Föster resonance for this state. Also, the relative spread in C_6 coefficients is much larger for the $5s63s$ ^{3}S states which probably reflects the importance for the hyperfine splitting to obtain such large C_6. Using the values of ν given in the caption, the eigenvalues in the figures can be converted to SI units: the $5s50s$ ^{1}S states have $C_6 \simeq -10.9$ GHz μm^6, the $5s50s$ ^{3}S states have $C_6 \simeq 30$ GHz μm^6, and the $5s63s$ ^{3}S states have $C_6 \sim 6 - 20$ THz μm^6. As with the polarizability calculations, we do not expect high accuracy for the $5s63s$ state but we do expect there to be large C_6 matrices in the neighborhood of this state.

As a test of the C_6 calculations, we computed the C_6 coefficient for the $5s50s$ ^{1}S state when setting the threshold splitting to 0 and compared that value to the tabulated results in [11] supplementary material. Our value was -6.792×10^{19} and [11] reported -6.820×10^{19}: a difference of 0.4%. We do not know the origin of this difference since we use the same quantum defects as [11] for both s-series and all of the p-series. We tried two different methods for calculating the radial matrix elements and found a difference more than a factor of 10 smaller than 0.4%. We also tried different convergence criteria in our sum over intermediate states, but, again, the change in our calculated value was too small to explain this difference.

4. Conclusions

We have calculated various energies, polarizabilities, and C_6 matrices of ^{87}Sr Rydberg states using a variation of the theory described in [13]. Because the quantum defects of Sr are known to much higher accuracy than the Ho example in [13] and the threshold structure is much simpler, we expect that the polarizabilities and C_6 coefficients of ^{87}Sr to be much more accurate than those for Ho. For example, the $5sns$ and

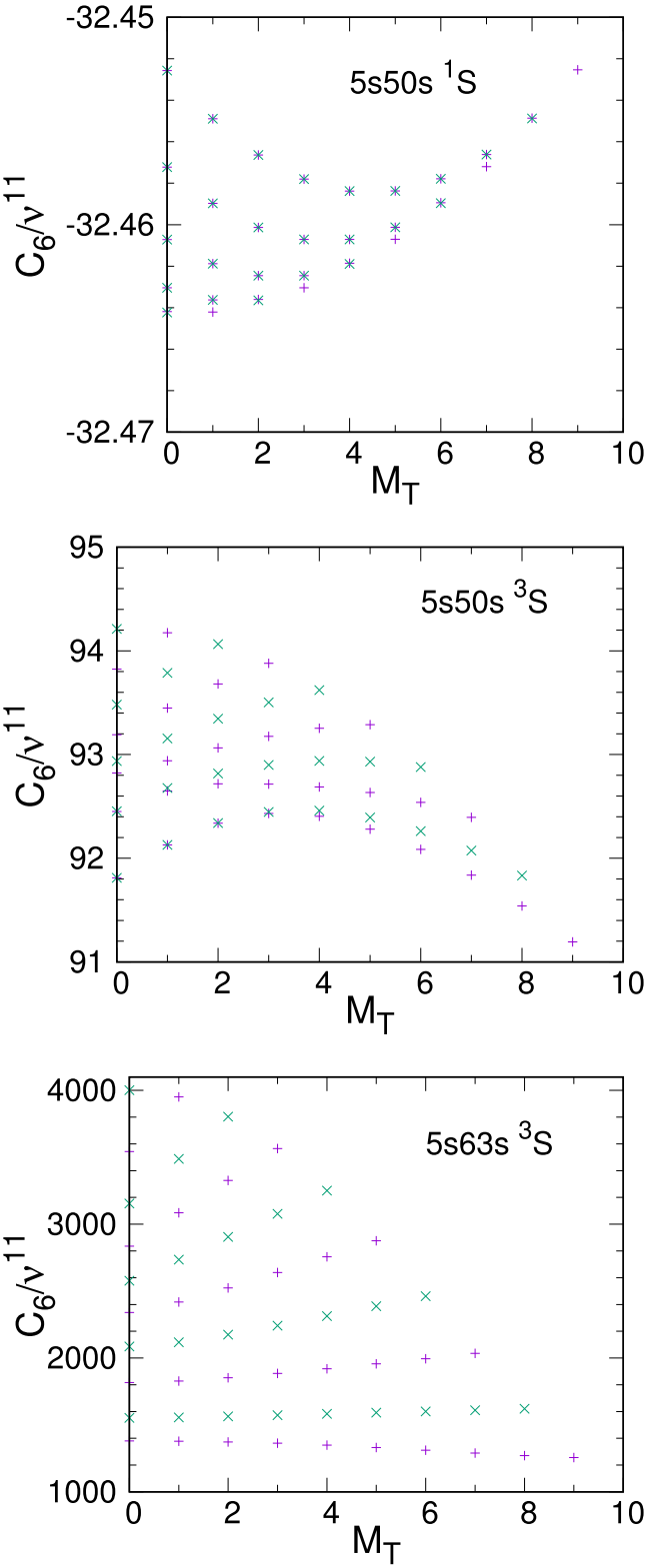

Figure 4. The eigenvalues of the C_6 matrix for three different states as a function of the total z-component of the angular momenta, $M_T = M_{T1} + M_{T2}$. The even state (+) and odd states (×) are plotted. To convert to GHz μm^6, multiply by 1.44×10^{-19}. The different values of ν are 46.744 429 for $5s50s$ ^{1}S, 46.623 502 for $5s50s$ ^{3}S, and 59.598 383 for $5s63s$ ^{3}S.

$5snp$ series are approaching the level of accuracy needed for quantitative predictions. In order to predict the C_6 matrix for the $5sns$ series more accurately, the most pressing measurement is of the $5snp$ quantum defects above $n = 50$. The values from [11] are obtained by a fit to levels $10 \leqslant n \leqslant 29$ for ^{1}P while the ^{3}P series has $8 \leqslant n \leqslant 15$, 22, and 18 for $J = 0$, 1, and 2 respectively.

Most importantly, the perturbations and energy shifts that arise due to the hyperfine splitting of the thresholds lead to strong enhancement of the polarizability and the C_6 coefficients that might not be present without the threshold splittings. This property is shared with the calculations in Ho which also has hyperfine split thresholds. Therefore, it should be possible to find many cases where the interactions between a pair of atoms is relatively strong. The relatively large C_6 interaction term could be useful for quantum simulators or computers.

In the case of the polarizability, the strong energy dependence leads to the polarizability changing sign with increasing n. This might be a useful feature because a state will have a small polarizability near the sign change. The smallest polarizability in figure 2 is at $n = 64.91$ with the value $\alpha_0 = -1.26 \times 10^{-3}\nu^7 = -4.23 \times 10^9$, much smaller than the $n = 50$ value of 9.13×10^{10}. States with anomalously small polarizabilities are somewhat protected from stray electric fields which might be useful for quantum simulators or computers.

Although the hyperfine split thresholds lead to more complicated Rydberg series, there appears to be possible advantages that make continued investigations worthwhile.

This work was supported by the National Science Foundation under Grant No. 1804026-PHY. We appreciate the data and communications with R Ding, TC Killian, and FB Dunning and appreciate TC Killian and MPA Jones for reading and commenting on a draft of this paper. We also appreciate physics discussions with CH Greene about problems associated with Sr and using quantum defects from different isotopes.

ORCID iDs

F Robicheaux https://orcid.org/0000-0002-8054-6040

References

[1] Gallagher T F 1994 *Rydberg Atoms* (Cambridge: Cambridge University Press)
[2] Daley A J, Boyd M M, Ye J and Zoller P 2008 Quantum computing with alkaline-earth-metal atoms *Phys. Rev. Lett.* **101** 170504
[3] Shibata K, Kato S, Yamaguchi A, Uetake S and Takahashi Y 2009 A scalable quantum computer with ultranarrow optical transition of ultracold neutral atoms in an optical lattice *Appl. Phys.* B **97** 753
[4] Mukherjee R, Millen J, Nath R, Jones M P A and Pohl T 2011 Many-body physics with alkaline-earth Rydberg lattices *J. Phys. B: At. Mol. Opt. Phys.* **44** 184010

[5] Topcu T and Derevianko A 2014 Divalent Rydberg atoms in optical lattices: Intensity landscape and magic trapping *Phys. Rev.* A **89** 023411
[6] Topcu T and Derevianko A 2016 Possibility of triple magic trapping of clock and Rydberg states of divalent atoms in optical lattices *J. Phys. B: At. Mol. Opt. Phys.* **49** 144004
[7] Millen J, Lochead G, Corbett G R, Potvliege R M and Jones M P A 2011 Spectroscopy of a cold strontium Rydberg gas *J. Phys. B: At. Mol. Opt. Phys.* **44** 184001
[8] Millen J, Lochead G and Jones M P A 2010 Two-electron excitation of an interacting cold rydberg gas *Phys. Rev. Lett.* **105** 213004
[9] Walker T G and Saffman M 2008 Consequences of Zeeman degeneracy for the van der Waals blockade between Rydberg atoms *Phys. Rev.* A **77** 032723
[10] Weber S, Tresp C, Menke H, Urvoy A, Firstenberg O, Büchler H P and Hofferberth S 2017 Calculation of Rydberg interaction potentials *J. Phys. B: At. Mol. Opt. Phys.* **50** 133001
[11] Vaillant C L, Jones M P A and Potvliege R M 2012 Long-range Rydber–Rydberg interactions in calcium, strontium and ytterbium *J. Phys. B: At. Mol. Opt. Phys.* **45** 135004
[12] Vaillant C L, Jones M P A and Potvliege R M 2014 Multichannel quantum defect theory of strontium bound Rydberg states *J. Phys. B: At. Mol. Opt. Phys.* **47** 155001
Vaillant C L, Jones M P A and Potvliege R M 2014 Multichannel quantum defect theory of strontium bound Rydberg states *J. Phys. B: At. Mol. Opt. Phys.* **47** 199601
[13] Robicheaux F, Booth D W and Saffman M 2018 Theory of long-range interactions for Rydberg states attached to hyperfine-split cores *Phys. Rev.* A **97** 022508
[14] Cooke W E, Gallagher T F, Edelstein S A and Hill R M 1978 Doubly excited autoionizing Rydberg states of Sr *Phys. Rev. Lett.* **40** 178
[15] Beigang R, Lücke K, Schmidt D, Timmermann A and West P J 1982 One-photon laser spectroscopy of Rydberg series from metastable levels in Calcium and Strontium *Phys. Scr.* **26** 183
[16] Beigang R, Makat W, Timmermann A and West P J 1983 Hyperfine-induced n mixing in high Rydberg states of ^{87}Sr *Phys. Rev. Lett.* **51** 771
[17] Sun J-Q and Lu K T 1988 Hyperfine structure of extremely high Rydberg msns $^1S_0$ and msns $^3S_1$ series in odd alkaline-earth isotopes *J. Phys. B: At. Mol. Opt. Phys.* **21** 1957
[18] Sun J-Q, Lu K T and Beigang R 1989 Hyperfine structure of extremely high Rydberg msnd $^1D_2$, $^3D_1$, $^3D_2$ and $^3D_3$ series in odd alkaline-earth isotopes *J. Phys. B: At. Mol. Opt. Phys.* **22** 2887
[19] Mauger S, Millen J and Jones M P A 2007 Spectroscopy of strontium Rydberg states using electromagnetically induced transparency *J. Phys. B: At. Mol. Opt. Phys.* **40** F319
[20] Aymar M, Greene C H and Luc-Koenig E 1996 Multichannel Rydberg spectroscopy of complex atoms *Rev. Mod. Phys.* **68** 1015
[21] Ye S, Zhang X, Killian T C, Dunning F B, Hiller M, Yoshida S, Nagele S and Burgdörfer J 2013 Production of very-high-n strontium rydberg atoms *Phys. Rev.* A **88** 043430
[22] Ding R, Whalen J D, Kanungo S K, Killian T C, Dunning F B, Yoshida S and Burgdörfer J 2018 Spectroscopy of Sr 87 triplet Rydberg states *Phys. Rev.* A **98** 042505
[23] Couturier L, Nosske I, Hu F, Tan C, Qiao C, Jiang Y H, Chen P and Weidemüller M 2019 Measurement of the strontium triplet Rydberg series by depletion spectroscopy of ultracold atoms *Phys. Rev.* A **99** 022503
[24] Sun J-Q 1989 Multichannel quantum defect theory of the hyperfine structure of high Rydberg states *Phys. Rev.* A **40** 7355
[25] Sunaoshi H, Fukashiro Y, Furukawa M, Yamauchi M, Hayashibe S, Shinozuka T, Fujioka M, Satoh I, Wada M and Matsuki S 1993 A precision measurement of the hyperfine structure of 87 Sr *Hyperfine Interact.* **78** 241–5
[26] de Laeter J R, Böhlke J K, De Bièvre P, Hidaka H, Peiser H S, Rosman K J R and Taylor P D P 2003 Atomic weights of the elements. Review 2000 (IUPAC Technical Report) *Pure Appl. Chem.* **75** 683
[27] Beigang R, Lücke K, Timmermann A, West P J and Frölich D 1982 Determination of absolute level energies of 5*sns* $^1s_0$ and 5*snd* $^1d_2$ Rydberg series of Sr *Opt. Commun.* **42** 19
[28] Rubbmark J R and Borgström S A 1978 Rydberg series in strontium found in absorption by selectively laser-excited atoms *Phys. Scr.* **18** 196
[29] Armstrong J A, Wynne J J and Esherick P 1979 Bound, odd-parity $j = 1$ spectra of the alkaline earths: Ca, Sr, and Ba *J. Opt. Soc. Am.* **69** 211
[30] Edmonds A R 1974 *Angular Momentum in Quantum Mechanics* 2nd edn (Princeton, NJ: Princeton University Press)
[31] Rose M E 1958 The electrostatic interaction of two arbitrary charge distributions *J. Math. Phys.* **37** 215
[32] Fontana P R 1961 Theory of long-range interatomic forces: I. Dispersion energies between unexcited atoms *Phys. Rev.* **123** 1865
[33] Dalgarno A and Davison W D 1966 The calculation of van der Waals interactions *Adv. At. Mol. Phys.* **2** 1